Geophysical Research Letters

RESEARCH LETTER
10.1029/2018GL078265

Strengthened Indonesian Throughflow Drives Decadal Warming in the Southern Indian Ocean

Ying Zhang[1,2,3], Ming Feng[3,4], Yan Du[1,2], Helen E. Phillips[5,6], Nathaniel L. Bindoff[5,6,7,8], and Michael J. McPhaden[9]

[1]State Key Laboratory of Tropical Oceanography, South China Sea Institute of Oceanology, Chinese Academy of Sciences, Guangzhou, China, [2]College of Earth Science, University of Chinese Academy of Sciences, Beijing, China, [3]CSIRO Oceans and Atmosphere, Crawley, Western Australia, Australia, [4]Centre for Southern Hemisphere Oceans Research, Hobart, Tasmania, Australia, [5]Institute for Marine and Antarctic Studies, University of Tasmania, Hobart, Tasmania, Australia, [6]ARC Centre of Excellence for Climate Systems Science, Hobart, Tasmania, Australia, [7]Antarctic Climate and Ecosystems Cooperative Research Centre, Hobart, Tasmania, Australia, [8]CSIRO Oceans and Atmosphere, Hobart, Tasmania, Australia, [9]NOAA Pacific Marine Environmental Laboratory, Seattle, WA, USA

Key Points:
- Upper-700 m temperature in the Southern Indian Ocean significantly increased during 1998–2015
- Enhanced heat advection and reduced net air-sea heat flux are responsible for the Southern Indian Ocean warming
- Increased Indonesian Throughflow heat transport is a main contributor to the Southern Indian Ocean warming during 1998–2015

Supporting Information:
- Figure S1
- Table S1

Correspondence to:
M. Feng,
ming.feng@csiro.au

Citation:
Zhang, Y., Feng, M., Du, Y., Phillips, H. E., Bindoff, N. L., & McPhaden, M. J. (2018). Strengthened Indonesian Throughflow drives decadal warming in the Southern Indian Ocean. *Geophysical Research Letters*, *45*, 6167–6175. https://doi.org/10.1029/2018GL078265

Received 16 APR 2018
Accepted 4 JUN 2018
Accepted article online 11 JUN 2018
Published online 22 JUN 2018

Abstract Remarkable warming of the Southern Indian Ocean during the recent two decades is assessed using a heat budget analysis based on the Estimating the Circulation and Climate of the Ocean version 4 release 3 model results. The annual mean temperature averaged in the upper-700 m Southern Indian Ocean during 1998–2015 has experienced significant warming at a rate of 1.03×10^{-2} °C/year. A heat budget analysis indicates that the increase is mostly driven by decreased cooling from net air-sea heat flux and increased warming from heat advection. Increased Indonesian Throughflow advection is the largest contributor to warming the upper 700 m of the Southern Indian Ocean, while the reduction of surface turbulent heat flux is of secondary importance. These results expand our understanding of the decadal heat balance in the Indian Ocean and of Indo-Pacific decadal climate variability.

Plain Language Summary This study identified the important role of the strengthened Indonesian Throughflow volume and heat transports during the global surface warming hiatus period in warming up the Southern Indian Ocean in the past two decades. Roles of other processes, such as air-sea heat fluxes, cross-equatorial cells, and the Agulhas Current, have also been quantified using the model. It appears that the heat transport anomaly is the dominant factor that drives the Southern Indian Ocean warming. Quantifying the decadal ocean heat balance is important to understand the redistribution of the anthropogenic heat uptake in the oceans. The results are useful in assessing coupled model performance in simulating climate change impacts on the global oceans. The study may have broad implications in the climate change research field, as well as the study of broad-scale oceanography, ocean circulation, and the Indonesian Throughflow.

1. Introduction

Global mean surface temperature warming slowed down sharply from the end of the twentieth century (Easterling & Wehner, 2009; Katsman & van Oldenborgh, 2011; Trenberth & Fasullo, 2013) despite the ever-increasing anthropogenic greenhouse gas concentrations (Allan et al., 2014; Fyfe et al., 2013; Kaufmann et al., 2011; Solomon et al., 2010). Recent studies have suggested that heat redistribution between the upper layers of the Pacific and Indian Oceans is closely tied to the hiatus in global mean surface temperature warming, because of increased heat transport from the Pacific to the Indian Ocean by the Indonesian Throughflow (ITF; Dong & McPhaden, 2016; England et al., 2014; Kosaka & Xie, 2013; Lee et al., 2015; Liu et al., 2016). The Southern Indian Ocean (SIO) upper ocean heat content has increased significantly during the hiatus period; however, a direct connection between the changes of the ITF heat transport and the ocean heat content of the SIO has not been quantified.

The ITF is a crucial component of the global overturning circulation, which carries warm seawater from the tropical Pacific to the Indian Ocean, impacting the mass and heat budgets of both the Pacific and Indian Oceans (Gordon, 1986; Gordon et al., 2010; Schneider, 1998). The ITF transport cools the Pacific, warms the Indian Ocean, and strengthens the South Equatorial Current and Agulhas Current (AC) in the Indian Ocean (Hirst & Godfrey, 1993). The ITF has a maximum (minimum) volume transport during austral winter

(summer; Wyrtki, 1987; Figures S2c, S2d, S3a, and S3b in the supporting information). Moreover, the ITF volume transport varies during the El Niño–Southern Oscillation (ENSO) cycle, being stronger during the La Niña phase and weaker during the El Niño phase (Clarke & Liu, 1994; Liu et al., 2015; Meyers, 1996). Recent studies demonstrated that ITF heat transport increased in the 2000s due to a series of long-lasting La Niña events without strong and intervening El Niño events (Li et al., 2017; Liu et al., 2015).

The Leeuwin Current (LC) and AC, the eastern and western boundary currents in the SIO, respectively, also play important roles in mass and heat budgets of the Indian Ocean and its adjacent oceans. The LC carries warm water poleward along the west coast of Australia, driven by the meridional pressure gradient setup by the ITF and the air-sea fluxes in the southeast Indian Ocean (Benthuysen et al., 2014; Furue et al., 2013; Thompson, 1984). The LC is strong in austral winter and weak in austral summer (Godfrey & Ridgway, 1985; Smith et al., 1991; Figures S2c, S2d, S3e, and S3f). The LC is stronger during the La Nina phase and weaker during the El Niño phase (Feng et al., 2003; Pearce & Phillips, 1988).

A large portion of the ITF transport eventually joins the AC on decadal timescales (Durgadoo et al., 2017). The AC is a narrow, swift, and strong current that carries warm water poleward along the eastern coast of Africa and is primarily forced by positive wind stress curl over the subtropical Indian Ocean (De Ruijter, 1982). The current is at a maximum during the austral summer and at a minimum during the austral winter (Matano et al., 1998; Figures S2c, S2d, S3e, and S3f). Recent studies suggested that the AC has not intensified but has broadened since the early 1990s, which could result in reduced poleward heat transport (Beal & Elipot, 2016).

The cross-equatorial cell also plays an important role in the SIO heat balance, as it provides the mass and heat exchange between the Northern and Southern Hemispheres in the Indian Ocean (Lee, 2004; Miyama et al., 2003; Schott et al., 2004, 2009). The cross-equatorial cell is a wind-driven circulation that carries warm Northern Hemisphere surface water southward across the equator to the SIO (Figures S2c, S2d, S3c, and S3d) where it subducts into the thermocline and flows northward to be upwelled off Somalia (Schott et al., 2009; Wang & McPhaden, 2017).

The changes in the upper Indian Ocean temperature over the past two decades have received increasing attention. Nieves et al. (2015) illustrated that the Indian Ocean 100–300 m depth layer has warmed significantly during 2003–2012. Lee et al. (2015) proposed that rapid increase in the top 700 m Indian Ocean heat content accounted for more than 70% of the global ocean upper-700 m heat content gain during 2003–2012. On the other hand, changes in the upper-700 m heat content of the Northern Indian Ocean are primarily attributed to changes in meridional heat transport across 5°S (Srinivasu et al., 2017; Thompson et al., 2016). The impacts of the ITF on heat content are speculated to be limited to the SIO (Srinivasu et al., 2017). The present study uses numerical simulations from an energy and momentum conserving data-assimilating model to study the decadal changes in temperature of the upper-700 m SIO and to quantify the relative importance of ITF transport and air-sea heat exchange on the SIO heat budget on decadal timescales.

2. Data and Methods

2.1. Estimating the Circulation and Climate of the Ocean version 4 release 3

The Estimating the Circulation and Climate of the Ocean version 4 release 3 (ECCO v4.3) is an optimal solution of Massachusetts Institute of Technology General Circulation Model (MITgcm; Marshall, Adcroft, et al., 1997; Marshall, Hill, et al., 1997), which is forced by an adjusted version of ERA-Interim atmospheric reanalysis (Dee et al., 2011). In the ECCO framework, the MITgcm is fit in a least squares sense to several hundred million (satellite and in situ) ocean observations (Forget et al., 2015; Wunsch & Heimbach, 2007; Wunsch et al., 2009). Each data point is weighted by a best-available estimate of its observational and representation error variance, and the least squares problem is solved by the method of Lagrange multipliers through iterative improvement relying upon a quasi-Newton gradient search (Gilbert & Lemaréchal, 1989). In addition, ECCO estimates satisfy the equations of motion and conservation laws without unidentified sources of heat and buoyancy (Wunsch & Heimbach, 2013); thus, they are dynamically and kinematically consistent, allowing us to explore the temperature changes and associated heat budget of the upper 700 m of the SIO during recent decades. The model has a truly global domain (including the Arctic) with 50 vertical layers, 1° zonal

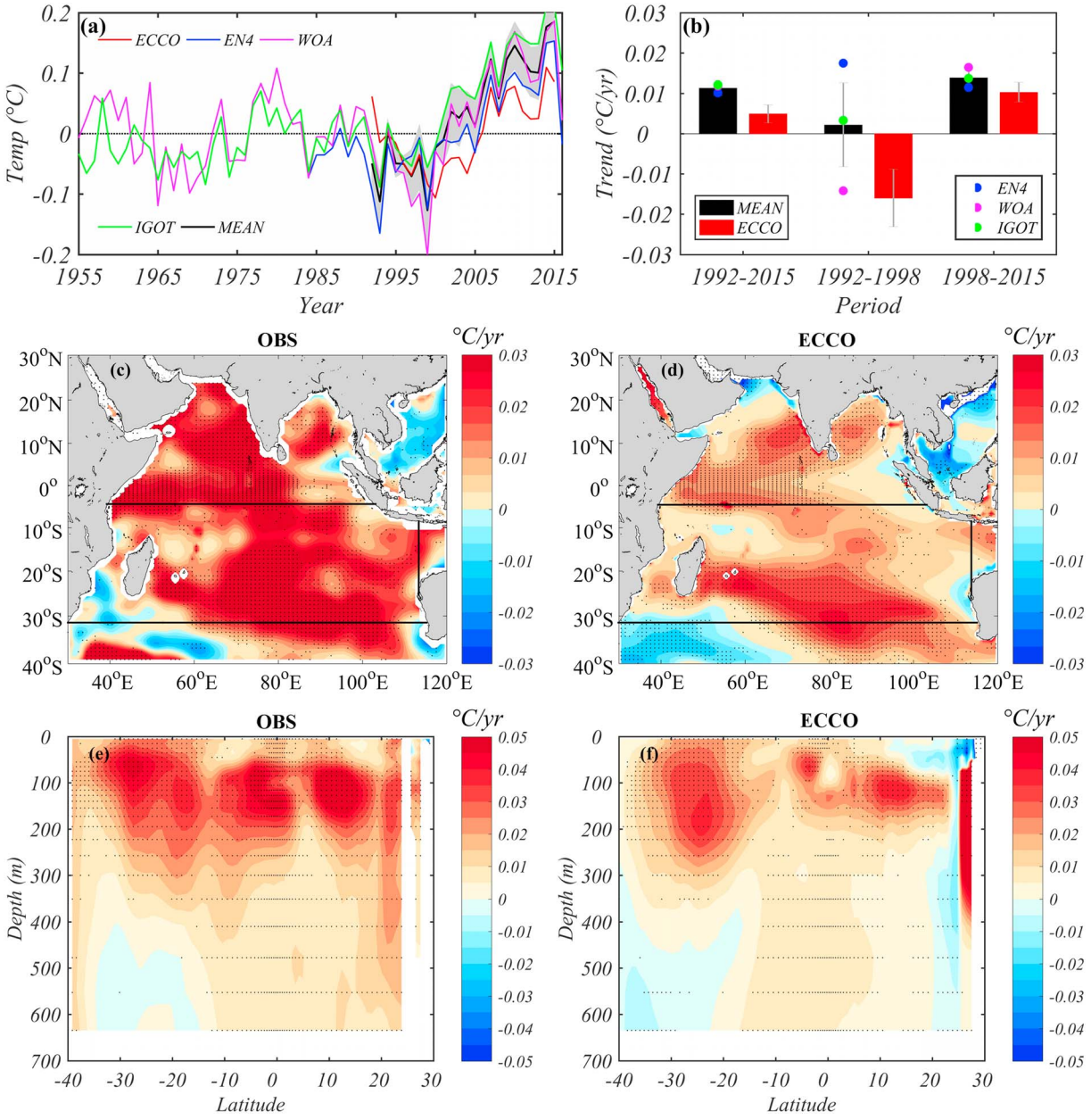

Figure 1. Temperature changes and linear trends. (a) Time series of annual mean temperature anomalies averaged in the upper-700 m of the SIO (32–5°S, Africa-115°E) from ECCO v4.3 (red), and three observational data sets: EN4 (blue), IGOTv3 (green), and WOA09 (magenta). The mean of the three observational data sets is shown in black with their spread indicated by gray shading. (b) Linear trends of the 0–700 m average temperature in the SIO from observations (black bars) and ECCO v4.3 (red bars) over periods 1992–2015, 1992–1998, and 1998–2015. The dots show the linear trend in temperature from the three observational data sets. The vertical error bars show the 90% confidence levels of the linear trends derived from regression coefficient confidence intervals based on bootstrap methods (Efron & Tibshirani, 1986). (c and d) Depth-averaged 0–700 m temperature trends during 1998–2015 from observations and ECCO v4.3, respectively, with the control volume for the heat budget shown in black lines. (e and f) Zonally averaged temperature trends for 1998–2015 over the Indian Ocean from observations and ECCO v4.3, respectively. The dotted areas in (c)–(f) indicate that the linear trends are statistically significant at the 95% confidence levels from a modified Mann-Kendall test.

resolution, and varying meridional resolution (approximately 1° at midlatitudes and 1/3° at the equator). The model simulation covers the period 1992–2015.

2.2. Observations

To estimate upper-ocean temperature changes in the SIO, objectively analyzed subsurface temperature fields from the ENACT/ENSEMBLES version 4 (EN4), World Ocean Atlas 2009 (WOA09), and the Institute of

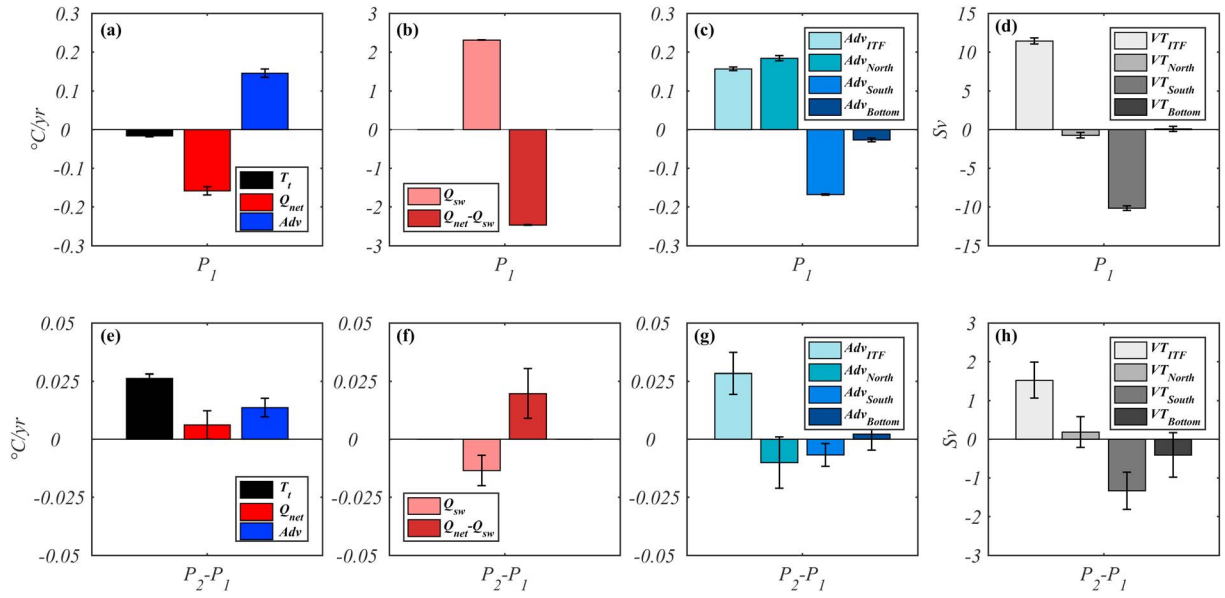

Figure 2. Mean values of (a) overall heat budget terms, (b) air-sea heat fluxes, (c) heat advection terms, and (d) volume transport for the Southern Indian Ocean during P_1. The difference between P_2 and P_1 of (e) overall heat budget terms, (f) air-sea heat fluxes, (g) heat advection terms, and (h) volume transport for the Southern Indian Ocean. Positive values mean into the control volume of the Southern Indian Ocean. The error bars in (a)–(h) represent one standard error based on a Student's *t* test.

Atmospheric Physics Global Ocean Temperature data set version 3 (IGOT) are used in this study. The monthly temperature fields from the EN4 database have a regular 1° horizontal grid and 42 levels in the vertical (Good et al., 2013; Levitus et al., 2009). WOA09 provides the yearly temperature anomaly fields, with a resolution of 1° × 1° and 16 levels in the upper 700 m (Levitus et al., 2012). The IGOT, mainly based on bias-corrected expendable bathythermograph (XBT) measurements from the World Ocean Database, has a resolution 1° × 1° and 41 levels in the upper 2,000 m (Cheng et al., 2017; Cheng & Zhu, 2016). In this study, we use the data sets from 1955 to 2016.

2.3. Heat Budget

The geographical domain chosen here to assess the SIO heat budget is the region between 32°S and 5°S, and bounded by the Eastern African coast in the west to 115°E and the Western Australian coast in the east. We choose 5°S as the northern limit of the control volume so as to include all the ITF transport from the east boundary. The temperature budget, equivalent to a heat budget by a constant factor, is formulated as

$$\frac{\partial}{\partial t}\left(\frac{\iiint_V T dV}{V}\right) = \mathrm{Adv} + \frac{1}{\rho C_\rho V}\iint_A Q_{\mathrm{net}} dxdy + \mathrm{Res} \tag{1}$$

$$\mathrm{Adv} = -\frac{1}{V}\left(\iint_{115°E} u(T-[T])dydz + \iint_{5°S} v(T-[T])dxdz - \iint_{32°S} v(T-[T])dxdz - \iint_{\mathrm{Area}} w_{-h}(T_{-h}-[T])dxdy\right) \tag{2}$$

$$[T] = \frac{\iiint_V T dV}{V} \tag{3}$$

where T is potential temperature; t is time; V and A are the volume and surface area of the domain, respectively; ρ (assumed constant at 1,025 kg/m^3) and C_p (assumed constant at 4,000 J · kg^{-1} · °C^{-1}) are the density and heat capacity of seawater; Q_{net} is the net air-sea heat flux, including solar radiation and the turbulent fluxes; and Res is the residual, which includes vertical mixing at the base of the control volume, set at 700 m, and all other unresolved vertical and horizontal processes. Adv is the integral of the resolved heat advection terms at the bottom boundary of the control volume at the depth of 700 m, and at the three horizontal open-ocean boundaries at 115°E (eastern boundary), 5°S (northern boundary), and 32°S (southern boundary). The velocity components (u, v, and w) are the zonal, meridional, and vertical

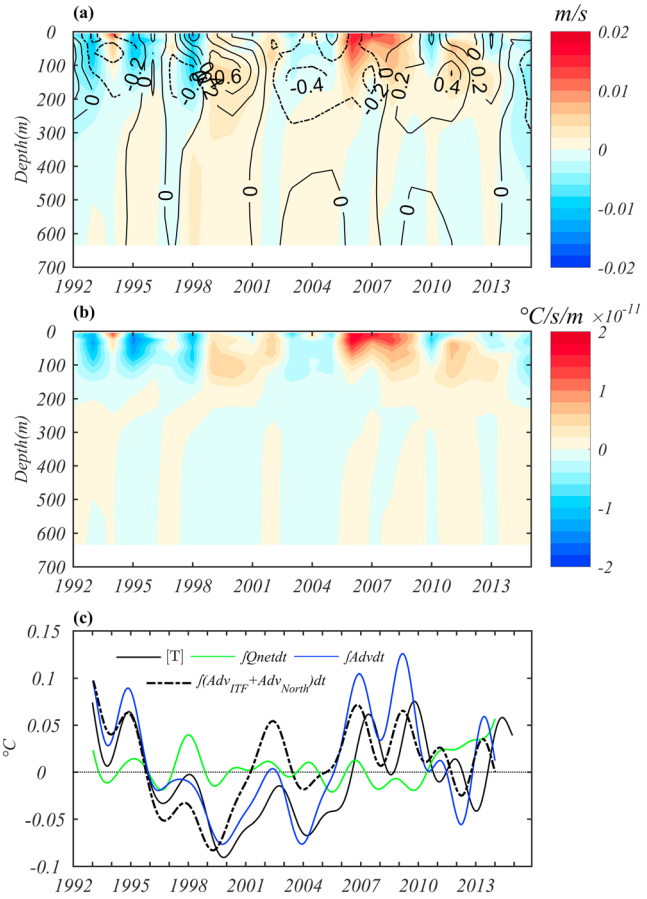

Figure 3. (a) Time-evolving annual mean relative temperature ($T - [T]$) anomalies (°C, contours) and velocity anomalies (m/s, shadings) averaged between 21° and 9°S along 115°E (ITF section) in the upper 700 m. (b) Time series of the meridional integral (21°–9°S) of anomalous heat advection across 115°E (ITF section) in the upper 700 m. (c) Averaged-temperature of the upper-700 m SIO ($[T]$, black); contribution of heat fluxes to $[T]$ ($\int Q_{net} dt$, green); contribution of heat advection to $[T]$ ($\int$Advdt, blue); contribution of ITF heat advection and heat advection across northern boundaries to $[T]$ ($\int \mathrm{Adv}_{ITF} dt + \int \mathrm{Adv}_{North} dt$, black dash). The mean and linear trend in (c) is removed.

velocities, respectively, including both geostrophic and Ekman currents. Here $[T]$ is the time variable but space-averaged potential temperature within the control volume, which is used as the reference temperature for the heat advection. By adding the $[T]$ in the heat advection terms, the external advection mechanisms that control the spatially averaged temperature of the domain including boundary processes are quantified. This allows us to distinguish external heat sources and sinks that control the spatially averaged temperature (Lee et al., 2004).

3. Changes in Temperature

Upper ocean temperature of the SIO has undergone significant decadal variations, with two significant warming periods, from mid-1960s to late 1970s, and after the late 1990s (Figure 1a; Zhou et al., 2017). The ECCO v4.3 model results well capture the observed decadal variations of temperature in the upper SIO (Figure 1a). The observed annual mean temperature shows weak to no increase during 1992–1998, while ECCO shows cooling due to a warmer than observed period around 1992 (Figure 1b). The intense interannual variability of temperature and the differences in magnitude of interannual variability among data sets lead to some differences in temperature change between the observations and model. However, the model and observations agree on an abrupt warming trend during 1998–2015. The linear trend of annual mean temperature during this period is 1.03×10^{-2} /year in the ECCOv4.3 simulation and 1.38×10^{-2} °C/year averaged across the three observational data sets (Figure 1b). Thus, significant upper ocean warming occurred in the SIO during 1998–2015.

In the following analysis we define two periods to quantify the rates of warming in the upper SIO, and the acceleration of warming since 1998. The reference period (P_1) is defined to be 1992–1998, and the warming period (P_2) is defined as 1998–2015. The warming during P_2 appeared in the whole upper SIO, albeit with spatial variations in magnitudes (Figures 1c and 1d). The zonally averaged warming extended to 700 m depth, with the strongest warming trapped within the thermocline layer (Figures 1e and 1f). The observed basin warming over the study region is well reproduced by the ECCO v4.3 despite quantitative differences in some areas (Figures 1c–1f).

4. Heat Budget Analysis

4.1. Seasonal Cycle of the Heat Balance

The volume transport into the control volume across the northern boundary shows a significant annual cycle, with a southward (northward) transport during austral winter (summer), which is dominated by the Ekman transport induced by the seasonally reversing monsoon winds (Figures S2a, S2b, S4a, and S4b; see also Wang & McPhaden, 2017). The volume transport across the eastern boundary (ITF transport) is positive all year-round, while the volume transport across the southern boundary is negative all year-round (Figure S4a).

The seasonal cycles of the heat advection follow the seasonal cycles of the volume transport, indicating the importance of the volume transport variations on the heat balance (Figures S4a and S4d). The heat advection across the northern boundary brings heat into the SIO during austral winter and exports heat northward out of the SIO during austral summer, which dominates the seasonal cycle of the total heat advection (Figure S4d). The ITF heat advection is positive all year-round, with an effect of warming the SIO, while the heat advection across the southern boundary is negative all year-round, with an effect of cooling the SIO (Figure S4d).

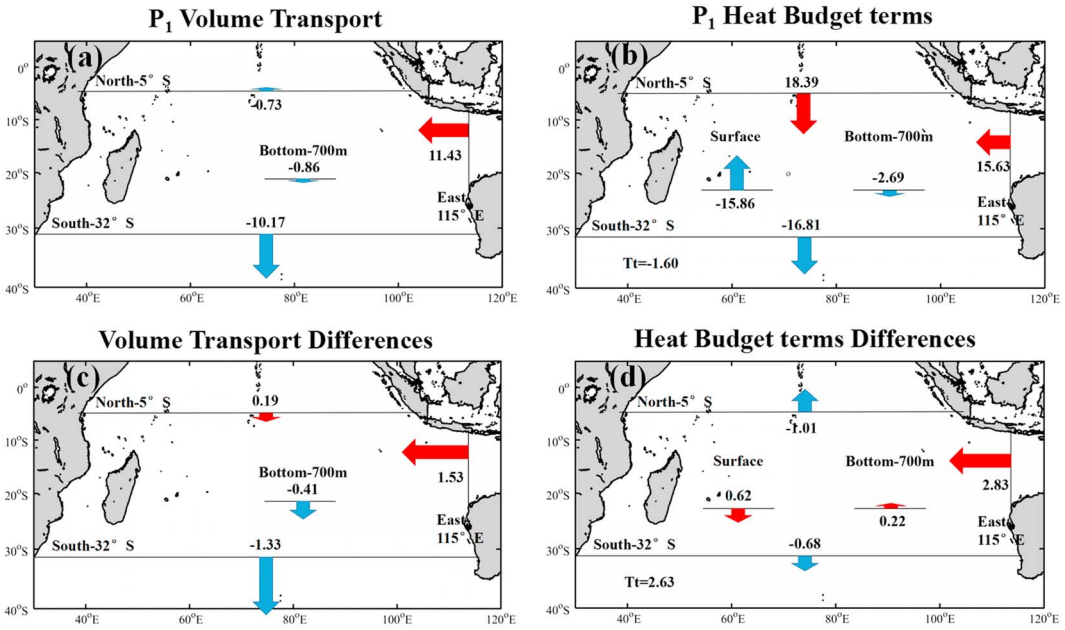

Figure 4. Average volume transport and heat budget balance for P_1 and their differences between P_2 and P_1: (a) the average volume transport across individual boundaries and (c) their differences; (b) the average heat budget terms and (d) their differences. In (a)–(d), the red arrows represent the heat and volume transport into the SIO and the blue arrows represent the heat and volume out from the SIO. Units in (a) and (c) are Sv; units in (b) and (d) are 10^{-2} °C/year.

The atmosphere heats the upper ocean of the SIO during October to March and cools the upper ocean during the rest of the year (Figure S4c). Thus, in response to the total heat advection and net air-sea heat flux forcing, the upper ocean cools during January to July, while it warms during August to December (Figure S4c).

4.2. Heat Balance Changes

The linear trend of annual mean temperature of the SIO was -1.61×10^{-2} °C/year (ECCO v4.3; Figure 1b) during P_1. The annual average net air-sea heat flux was directed from the ocean into the atmosphere (Figure 2a), while the total heat advection carries heat into the SIO (Figure 2a). These two terms—advection and surface fluxes—dominate the heat balance in the upper-700 m SIO during P_1 (Figure 2a). The residual term has a small warming contribution to the heat balance (not shown).

On average, the ITF heat advection and heat advection across the northern boundary have notable warming contributions to the heat balance, carrying heat into the SIO through the ITF and Ekman transports, respectively (Figures 2c and 2d and S5a and S5b). The heat advection across the southern boundary, however, removes heat from the SIO, predominantly via the southward AC (Figures 2c and S6a and S6b). Overall, the upper ocean of the SIO gains heat from heat advection. The cooling effect of vertical heat advection on the upper-700 m SIO is relatively small (Figure 2c). The annual average net air-sea heat flux has remarkable cooling contribution to the heat balance of the upper SIO, as the cooling effect of the surface turbulent heat flux is stronger than the warming effect of the shortwave radiation (Figures 2c and S7a, S7c, and S7e).

Compared with the annual average heat balance terms during the reference period P_1, the cooling effect of the net air-sea heat flux weakened and the warming impact of the total heat advection strengthened during P_2. This combination resulted in the increase in upper ocean temperature of the SIO during P_2 (Figure 2e).

The enhanced ITF heat advection is the largest contributor to the upper ocean warming in the SIO (Figure 2g), due to positive heat transport anomalies that result from anomalously strong transports into the SIO of anomalously warm waters during P_2 (Figures 3a and 3b). To further understand the contributions of ocean circulation and air-sea heat flux to the temperature changes on decadal timescales, the temporal integrals of the heat advection and air-sea heat flux terms are shown in Figure 3c. The time integral of the ITF heat advection and heat advection across the northern boundary dominates the temperature changes in the upper-700 m SIO (Figure 3c). In particular, the ITF heat advection has robust decadal variations, which is

consistent with decadal changes in temperature of the upper-700 m SIO (Figure S8). However, the heat advection across the northern boundary may play an opposing role (Figure S8). The heat advection across the northern boundary decreased, carrying less warm water southward into the SIO (Figures 2g and S5c and S5d), because of the subdued Ekman transport associated with the weakened monsoon winds over the North Indian Ocean (Srinivasu et al., 2017; Thompson et al., 2016). The heat advection across the southern boundary also has a cooling contribution, with increased poleward heat transport, caused by the broadened AC and intensified LC (Figures 2g and S6c and S6d; Beal & Elipot, 2016; Feng et al., 2016). The cooling effect of the vertical heat advection weakened, which has a warming contribution that is small in comparison to the other terms (Figure 2g).

The contribution of net air-sea surface heat flux shows less decadal-scale variation compared to the advective contributions (Figure 3c). Comparing P_2 with P_1, the decreased surface turbulent heat flux contributes to warming the upper SIO, while the decreased shortwave radiation cools the upper SIO (Figures 2f and S7d and S7f). Overall, the anomalous surface turbulent heat flux dominated over the anomalous shortwave radiation, and the changes in the net air-sea heat flux pattern, is similar to that in the surface turbulent heat flux (Figures S7b, S7d, and S7f). The surface turbulent heat flux anomalies are in part due to the weakened trade winds in the SIO (Figure S7d).

5. Conclusions and Discussion

In this study, monthly model output of ECCO v4.3 is used to investigate the roles of ITF transport in the decadal warming of the SIO during 1998–2015. In the SIO, the significant seasonal cycle of total heat advection is dominated by the monsoon-driven Ekman transport across 5°S. On average, the upper ocean heat budget is balanced between warm horizontal advection from the Ekman flow across 5°S and the ITF, and the cooling effect at the air-sea interface (Figure 4b). Compared with the heat balance during 1992–1998, a significant warming trend is found in the upper 700 m of the SIO during 1998–2015. The decadal changes of temperature in the upper-700 m SIO during this period are dominated by the increased warming contribution of the heat advection. ITF heat advection is the largest contributor and drives the temperature changes in the upper-700 m of the SIO; the surface turbulent heat flux anomalies have a secondary contribution to the SIO warming during this period (Figure 4d).

Positive heat transport anomalies of the ITF occurred frequently during 1998–2015 (Figure 3b), which correspond to the more frequent La Nina events associated with the negative phase of the IPO (Lee et al., 2015; Liu et al., 2015; Sprintall & Révelard, 2014). Thus, a significant trend of increased ITF heat transport is evident during 1992–2015 (Figure 3b), which is related to intensifying trade winds over the tropical Pacific since the early 1990s (England et al., 2014; Liu et al., 2015; Sprintall & Révelard, 2014). We note that the transport and temperature anomalies are mostly confined in the upper 700 m; thus, the good comparison between the ITF transport variability derived from the IX1 XBT line (Liu et al., 2015) and the ECCO model essentially supports the main conclusion from this study (Figure S9).

The relative contributions of heat advection and air-sea heat flux to the decadal warming in the SIO vary with the selection of the depth of the control volume in the ECCO model (Table S2). Seven hundred meters is the optimal depth for examining the integrated changes in upper ocean heat content associated with the redistribution of heat between the Pacific and Indian Oceans linked to the recent hiatus in global mean surface temperature warming. We note that the ECCO model may have underestimated the decadal warming trend in the SIO during 1998–2015. The discrepancies between ECCO results and other data sets, as well as the difference among various data sets, warrant further study.

It is evident that a complete understanding of climate variability and change will require an ability to robustly assess changes like those observed over the past two decades in the Indo-Pacific region. Using the ECCO model output (Bowen et al., 2017; Buckley et al., 2014; Thompson et al., 2016), we found that the ITF plays a major role in climate variations of global consequence. The ITF, however, may experience a substantial decrease in the future based on climate models and ocean downscaling models (Feng et al., 2017; Sen Gupta et al., 2016). Thus, it is important not only to sustain existing broad scale ocean observing systems for climate in the Indian and Pacific Oceans but to establish sustained observing systems for ocean boundary currents that define the major pathways of ITF-related transport. Only in this way will be able to thoroughly

evaluate the impacts of Indo-Pacific ocean circulation on climate variability and change, both regionally and globally.

Acknowledgments
This study is supported by the National Natural Science Foundation of China (41525019), the State Oceanic Administration of China (GASI-IPOVAI-02), the Centre for Southern Hemisphere Oceans Research (CSHOR), and the China Scholarship Council. CSHOR is a joint initiative between the Qingdao National Laboratory for Marine Science and Technology (QNLM), CSIRO, University of New South Wales, and University of Tasmania. This work is also supported by the CAS/SAFEA International Partnership Program for Creative Research Teams. The authors would like to thank the data providers that make this work possible. ECCO v4.3 fields can be downloaded here ftp://mit.ecco-group.org/ecco_for_las/version_4/release2/. EN4 temperature field is provided from Met Office Hadley Centre (http://www.metoffice.gov.uk/hadobs/en4/download-en4-2-0.html). IGOTv3 temperature field was obtained from Lijing Cheng's website (http://159.226.119.60/cheng/). WOA09 is available at https://www.nodc.noaa.gov/OC5/3M_HEAT_CONTENT/anomaly_data.html. H. P. and N. B. acknowledge support from the Australian Government Department of the Environment and Energy National Environmental Science Program. We thank QinYan Liu for providing the ITF transport derived from XBT data. This is PMEL contribution number 4775.

References

Allan, R. P., Liu, C., Loeb, N. G., Palmer, M. D., Roberts, M., Smith, D., & Vidale, P. L. (2014). Changes in global net radiative imbalance 1985–2012. *Geophysical Research Letters*, *41*, 5588–5597. https://doi.org/10.1002/2014GL060962

Beal, L. M., & Elipot, S. (2016). Broadening not strengthening of the Agulhas Current since the early 1990s. *Nature*, *540*(7634), 570–573. https://doi.org/10.1038/nature19853

Benthuysen, J., Furue, R., McCreary, J. P., Bindoff, N. L., & Phillips, H. E. (2014). Dynamics of the Leeuwin Current: Part 2. Impacts of mixing, friction, and advection on a buoyancy-driven eastern boundary current over a shelf. *Dynamics of Atmospheres and Oceans*, *65*, 39–63. https://doi.org/10.1016/j.dynatmoce.2013.10.004

Bowen, M., Markham, J., Sutton, P., Zhang, X., Wu, Q., Shears, N. T., & Fernandez, D. (2017). Interannual variability of sea surface temperature in the Southwest Pacific and the role of ocean dynamics. *Journal of Climate*, *30*(18), 7481–7492. https://doi.org/10.1175/JCLI-D-16-0852.1

Buckley, M. W., Ponte, R. M., Forget, G., & Heimbach, P. (2014). Low-frequency SST and upper-ocean heat content variability in the North Atlantic. *Journal of Climate*, *27*(13), 4996–5018. https://doi.org/10.1175/JCLI-D-13-00316.1

Cheng, L., Trenberth, K. E., Fasullo, J., Boyer, T., Abraham, J., & Zhu, J. (2017). Improved estimates of ocean heat content from 1960 to 2015. *Science Advances*, *3*(3), e1601545. https://doi.org/10.1126/sciadv.1601545

Cheng, L., & Zhu, J. (2016). Benefits of CMIP5 multimodel ensemble in reconstructing historical ocean subsurface temperature variations. *Journal of Climate*, *29*(15), 5393–5416. https://doi.org/10.1175/JCLI-D-15-0730.1

Clarke, A. J., & Liu, X. (1994). Interannual sea level in the northern and eastern Indian Ocean. *Journal of Physical Oceanography*, *24*(6), 1224–1235. https://doi.org/10.1175/1520-0485(1994)024<1224:ISLITN>2.0.CO;2

De Ruijter, W. (1982). Asymptotic analysis of the Agulhas and Brazil Current systems. *Journal of Physical Oceanography*, *12*(4), 361–373. https://doi.org/10.1175/1520-0485(1982)012<0361:AAOTAA>2.0.CO;2

Dee, D. P., Uppala, S., Simmons, A., Berrisford, P., Poli, P., Kobayashi, S., et al. (2011). The ERA-Interim reanalysis: Configuration and performance of the data assimilation system. *Quarterly Journal of the Royal Meteorological Society*, *137*(656), 553–597. https://doi.org/10.1002/qj.828

Dong, L., & McPhaden, M. (2016). Interhemispheric SST gradient trends in the Indian Ocean prior to and during the recent global warming Hiatus. *Journal of Climate*, *29*(24), 9077–9095. https://doi.org/10.1175/JCLI-D-16-0130.1

Durgadoo, J. V., Rühs, S., Biastoch, A., & Böning, C. W. (2017). Indian Ocean sources of Agulhas leakage. *Journal of Geophysical Research: Oceans*, *122*, 3481–3499. https://doi.org/10.1002/2016JC012676

Easterling, D. R., & Wehner, M. F. (2009). Is the climate warming or cooling? *Geophysical Research Letters*, *36*, L08706. https://doi.org/10.1029/2009GL037810

Efron, B., & Tibshirani, R. J. (1986). Bootstrap methods for standard errors, confidence intervals and other measures of statistical accuracy. *Statistical Science*, *1*, 54–77.

England, M. H., McGregor, S., Spence, P., Meehl, G. A., Timmermann, A., Cai, W., et al. (2014). Recent intensification of wind-driven circulation in the Pacific and the ongoing warming hiatus. *Nature Climate Change*, *4*(3), 222–227. https://doi.org/10.1038/nclimate2106

Feng, M., Meyers, G., Pearce, A., & Wijffels, S. (2003). Annual and interannual variations of the Leeuwin Current at 32°S. *Journal of Geophysical Research*, *108*(C11), 3355. https://doi.org/10.1029/2002JC001763

Feng, M., Zhang, X., Oke, P., Monselesan, D., Chamberlain, M., Matear, R., & Schiller, A. (2016). Invigorating ocean boundary current systems around Australia during 1979–2014: As simulated in a near-global eddy-resolving ocean model. *Journal of Geophysical Research: Oceans*, *121*, 3395–3408. https://doi.org/10.1002/2016JC011842

Feng, M., Zhang, X., Sloyan, B., & Chamberlain, M. (2017). Contribution of the deep ocean to the centennial changes of the Indonesian Throughflow. *Geophysical Research Letters*, *44*, 2859–2867. https://doi.org/10.1002/2017GL072577

Forget, G., Campin, J.-M., Heimbach, P., Hill, C., Ponte, R., & Wunsch, C. (2015). ECCO version 4: An integrated framework for non-linear inverse modeling and global ocean state estimation. *Geoscientific Model Development*, *8*(10), 3071–3104. https://doi.org/10.5194/gmd-8-3071-2015

Furue, R., McCreary, J. P., Benthuysen, J., Phillips, H. E., & Bindoff, N. L. (2013). Dynamics of the Leeuwin Current: Part 1. Coastal flows in an inviscid, variable-density, layer model. *Dynamics of Atmospheres and Oceans*, *63*, 24–59. https://doi.org/10.1016/j.dynatmoce.2013.03.003

Fyfe, J. C., von Salzen, K., Cole, J. N. S., Gillett, N. P., & Vernier, J. P. (2013). Surface response to stratospheric aerosol changes in a coupled atmosphere–ocean model. *Geophysical Research Letters*, *40*, 584–588. https://doi.org/10.1002/grl.50156

Gilbert, J. C., & Lemaréchal, C. (1989). Some numerical experiments with variable-storage quasi-Newton algorithms. *Mathematical Programming*, *45*(1-3), 407–435. https://doi.org/10.1007/BF01589113

Godfrey, J., & Ridgway, K. (1985). The large-scale environment of the poleward-flowing Leeuwin Current, Western Australia: Longshore steric height gradients, wind stresses and geostrophic flow. *Journal of Physical Oceanography*, *15*(5), 481–495. https://doi.org/10.1175/1520-0485(1985)015<0481:TLSEOT>2.0.CO;2

Good, S. A., Martin, M. J., & Rayner, N. A. (2013). EN4: Quality controlled ocean temperature and salinity profiles and monthly objective analyses with uncertainty estimates. *Journal of Geophysical Research: Oceans*, *118*, 6704–6716. https://doi.org/10.1002/2013JC009067

Gordon, A., Sprintall, J., Van Aken, H., Susanto, D., Wijffels, S., Molcard, R., et al. (2010). The Indonesian Throughflow during 2004–2006 as observed by the INSTANT program. *Dynamics of Atmospheres and Oceans*, *50*(2), 115–128. https://doi.org/10.1016/j.dynatmoce.2009.12.002

Gordon, A. L. (1986). Interocean exchange of thermocline water. *Journal of Geophysical Research*, *91*(C4), 5037–5046. https://doi.org/10.1029/JC091iC04p05037

Hirst, A. C., & Godfrey, J. (1993). The role of Indonesian Throughflow in a global ocean GCM. *Journal of Physical Oceanography*, *23*(6), 1057–1086. https://doi.org/10.1175/1520-0485(1993)023<1057:TROITI>2.0.CO;2

Katsman, C. v., & van Oldenborgh, G. J. (2011). Tracing the upper ocean's "missing heat". *Geophysical Research Letters*, *38*, L14610. https://doi.org/10.1029/2011GL048417

Kaufmann, R. K., Kauppi, H., Mann, M. L., & Stock, J. H. (2011). Reconciling anthropogenic climate change with observed temperature 1998–2008. *Proceedings of the National Academy of Sciences of the United States of America*, *108*(29), 11,790–11,793. https://doi.org/10.1073/pnas.1102467108

Kosaka, Y., & Xie, S.-P. (2013). Recent global-warming hiatus tied to equatorial Pacific surface cooling. *Nature*, *501*(7467), 403–407. https://doi.org/10.1038/nature12534

Lee, S.-K., Park, W., Baringer, M. O., Gordon, A. L., Huber, B., & Liu, Y. (2015). Pacific origin of the abrupt increase in Indian Ocean heat content during the warming hiatus. *Nature Geoscience*, *8*(6), 445–449. https://doi.org/10.1038/ngeo2438

Lee, T. (2004). Decadal weakening of the shallow overturning circulation in the South Indian Ocean. *Geophysical Research Letters*, *31*, L22302. https://doi.org/10.1029/2004GL021774

Lee, T., Fukumori, I., & Tang, B. (2004). Temperature advection: Internal versus external processes. *Journal of Physical Oceanography*, *34*(8), 1936–1944. https://doi.org/10.1175/1520-0485(2004)034<1936:TAIVEP>2.0.CO;2

Levitus, S., Antonov, J. I., Boyer, T. P., Baranova, O. K., Garcia, H. E., Locarnini, R. A., et al. (2012). World ocean heat content and thermosteric sea level change (0–2000 m), 1955–2010. *Geophysical Research Letters*, *39*, L10603. https://doi.org/10.1029/2012GL051106

Levitus, S., Antonov, J. I., Boyer, T. P., Locarnini, R. A., Garcia, H. E., & Mishonov, A. V. (2009). Global ocean heat content 1955–2008 in light of recently revealed instrumentation problems. *Geophysical Research Letters*, *36*, L07608. https://doi.org/10.1029/2008GL037155

Li, Y., Han, W., & Zhang, L. (2017). Enhanced decadal warming of the southeast Indian Ocean during the recent global surface warming slowdown. *Geophysical Research Letters*, *44*, 9876–9884. https://doi.org/10.1002/2017GL075050

Liu, Q. Y., Feng, M., Wang, D., & Wijffels, S. (2015). Interannual variability of the Indonesian Throughflow transport: A revisit based on 30 year expendable bathythermograph data. *Journal of Geophysical Research: Oceans*, *120*, 8270–8282. https://doi.org/10.1002/2015JC011351

Liu, W., Xie, S.-P., & Lu, J. (2016). Tracking ocean heat uptake during the surface warming hiatus. *Nature Communications*, *7*, 10926. https://doi.org/10.1038/ncomms10926

Marshall, J., Adcroft, A., Hill, C., Perelman, L., & Heisey, C. (1997). A finite-volume, incompressible Navier Stokes model for studies of the ocean on parallel computers. *Journal of Geophysical Research*, *102*(C3), 5753–5766. https://doi.org/10.1029/96JC02775

Marshall, J., Hill, C., Perelman, L., & Adcroft, A. (1997). Hydrostatic, quasi-hydrostatic, and nonhydrostatic ocean modeling. *Journal of Geophysical Research*, *102*(C3), 5733–5752. https://doi.org/10.1029/96JC02776

Matano, R. P., Simionato, C., De Ruijter, W., Van Leeuween, P., Strub, P. T., Chelton, D. B., & Schlax, M. (1998). Seasonal variability in the Agulhas Retroflection region. *Geophysical Research Letters*, *25*(23), 4361–4364. https://doi.org/10.1029/1998GL900163

Meyers, G. (1996). Variation of Indonesian Throughflow and the El Niño-Southern Oscillation. *Journal of Geophysical Research*, *101*(C5), 12,255–12,263. https://doi.org/10.1029/95JC03729

Miyama, T., McCreary, J. P., Jensen, T. G., Loschnigg, J., Godfrey, S., & Ishida, A. (2003). Structure and dynamics of the Indian-Ocean cross-equatorial cell. *Deep Sea Research Part II: Topical Studies in Oceanography*, *50*(12-13), 2023–2047. https://doi.org/10.1016/S0967-0645(03)00044-4

Nieves, V., Willis, J. K., & Patzert, W. C. (2015). Recent hiatus caused by decadal shift in indo-Pacific heating. *Science*, *349*(6247), 532–535. https://doi.org/10.1126/science.aaa4521

Pearce, A., & Phillips, B. (1988). ENSO events, the Leeuwin Current, and larval recruitment of the western rock lobster. *ICES Journal of Marine Science*, *45*(1), 13–21. https://doi.org/10.1093/icesjms/45.1.13

Schneider, N. (1998). The Indonesian Throughflow and the global climate system. *Journal of Climate*, *11*(4), 676–689. https://doi.org/10.1175/1520-0442(1998)011<0676:TITATG>2.0.CO;2

Schott, F. A., Mccreary, J. P., & Johnson, G. C. (2004). Shallow overturning circulations of the tropical-subtropical oceans. *Earth's Climate*, 261–304.

Schott, F. A., Xie, S. P., & McCreary, J. P. (2009). Indian Ocean circulation and climate variability. *Reviews of Geophysics*, *47*, RG1002. https://doi.org/10.1029/2007RG000245

Sen Gupta, A., McGregor, S., Sebille, E., Ganachaud, A., Brown, J. N., & Santoso, A. (2016). Future changes to the Indonesian Throughflow and Pacific circulation: The differing role of wind and deep circulation changes. *Geophysical Research Letters*, *43*, 1669–1678. https://doi.org/10.1002/2016GL067757

Smith, R. L., Huyer, A., Godfrey, J. S., & Church, J. A. (1991). The Leeuwin current off western Australia, 1986–1987. *Journal of Physical Oceanography*, *21*(2), 323–345. https://doi.org/10.1175/1520-0485(1991)021<0323:TLCOWA>2.0.CO;2

Solomon, S., Rosenlof, K. H., Portmann, R. W., Daniel, J. S., Davis, S. M., Sanford, T. J., & Plattner, G.-K. (2010). Contributions of stratospheric water vapor to decadal changes in the rate of global warming. *Science*, *327*(5970), 1219–1223. https://doi.org/10.1126/science.1182488

Sprintall, J., & Révelard, A. (2014). The Indonesian Throughflow response to Indo-Pacific climate variability. *Journal of Geophysical Research: Oceans*, *119*, 1161–1175. https://doi.org/10.1002/2013JC009533

Srinivasu, U., Ravichandran, M., Han, W., Sivareddy, S., Rahman, H., Li, Y., & Nayak, S. (2017). Causes for the reversal of North Indian Ocean decadal sea level trend in recent two decades. *Climate Dynamics*, 1–18.

Thompson, P., Piecuch, C., Merrifield, M., McCreary, J., & Firing, E. (2016). Forcing of recent decadal variability in the equatorial and North Indian Ocean. *Journal of Geophysical Research: Oceans*, *121*, 6762–6778. https://doi.org/10.1002/2016JC012132

Thompson, R. O. (1984). Observations of the Leeuwin current off Western Australia. *Journal of Physical Oceanography*, *14*(3), 623–628. https://doi.org/10.1175/1520-0485(1984)014<0623:OOTLCO>2.0.CO;2

Trenberth, K. E., & Fasullo, J. T. (2013). An apparent hiatus in global warming? *Earth's Future*, *1*(1), 19–32. https://doi.org/10.1002/2013EF000165

Wang, Y., & McPhaden, M. J. (2017). Seasonal cycle of cross-equatorial flow in the central Indian Ocean. *Journal of Geophysical Research: Oceans*, *122*, 3817–3827. https://doi.org/10.1002/2016JC012537

Wunsch, C., & Heimbach, P. (2007). Practical global oceanic state estimation. *Physica D: Nonlinear Phenomena*, *230*(1-2), 197–208. https://doi.org/10.1016/j.physd.2006.09.040

Wunsch, C., & Heimbach, P. (2013). Dynamically and kinematically consistent global ocean circulation and ice state estimates. In G. Siedler, S. M. Griffies, J. Gould, & J. A. Church (Eds.), *Ocean Circulation and Climate: A 21 Century Perspective: A 21 Century Perspective* (Vol. 103, pp. 553–579). Oxford, UK: Academic Press.

Wunsch, C., Heimbach, P., Ponte, R. M., Fukumori, I., & Members, E.-G. C. (2009). The global general circulation of the ocean estimated by the ECCO-Consortium. *Oceanography*, *22*(2), 88–103. https://doi.org/10.5670/oceanog.2009.41

Wyrtki, K. (1987). Indonesian through flow and the associated pressure gradient. *Journal of Geophysical Research*, *92*(C12), 12,941–12,946. https://doi.org/10.1029/JC092iC12p12941

Zhou, X., Alves, O., Marsland, S. J., Bi, D., & Hirst, A. C. (2017). Multi-decadal variations of the South Indian Ocean subsurface temperature influenced by Pacific Decadal Oscillation. *Tellus A: Dynamic Meteorology and Oceanography*, *69*(1), 1308055. https://doi.org/10.1080/16000870.2017.1308055